Effects of hybridization on the tension–tension fatigue behavior of continuous-discontinuous fiber-reinforced sheet molding compound composites

M. Bartkowiak [a,*], W.V. Liebig [a], J. Montesano [b], K.A. Weidenmann [c]

[a] Karlsruhe Institute of Technology, Institute for Applied Materials – Material Science and Engineering, Kaiserstr. 12, 76131 Karlsruhe, Germany
[b] Composites Research Group, University of Waterloo, Department of Mechanical and Mechatronics Engineering, 200 University Ave. West, N2L 3G1 Waterloo, Canada
[c] University of Augsburg, Institute for Materials Resource Management, Am Technologiezentrum 8, 86159 Augsburg, Germany

ABSTRACT

This study is focused on the fatigue of sheet molding compounds (SMC) with a discontinuous (DiCo) glass fiber-reinforced core and continuous (Co) unidirectional ([0/DiCo/0]) or cross-ply ([0/90/DiCo/90/0]) carbon fiber-reinforced face layers. Tension-tension tests were conducted on the constituents (i.e., DiCo and Co SMC) and hybrid specimens. Hybridization effects were larger under cyclic than under monotonic loading. Constraining effects resulted in enhanced high fatigue strength of the Co plies in [0/DiCo/0]. [0/90/DiCo/90/0] was more sensitive to fatigue than [0/DiCo/0] due to localized damage starting from 90°-ply cracks. The S-N behavior of the hybrid was approximated from the behavior of DiCo SMC.

1. Introduction

Discontinuous fiber-reinforced sheet molding compounds (SMC) have been well-established as non-structural and semi-structural components in the automotive industry. SMCs offer the possibility to manufacture complex shaped parts through compression molding processes, which cannot be realized with continuous fiber reinforcements. Design freedom resulting from the flowability of SMC combined with low production costs makes this material system attractive for high volume production automobiles. However, their mechanical properties are considerably lower than those of continuous fiber-reinforced composites due to their limited fiber length, which prevents their use in structural components. One approach to overcome this disadvantage is the combination of discontinuous fiber-reinforced SMC with a load-optimized continuous fiber reinforcement [1]. An example for an application of such a hybrid material system is a subframe made of continuous and chopped carbon fiber-reinforced SMC combined in a co-molding process [2]. Another application in the automotive sector involves the use of chopped glass and carbon fiber SMC combined with unidirectional carbon fiber reinforcement to fabricate a windshield surround [3]. The structural complexity of hybrid continuous-discontinuous fiber-reinforced composites presents challenges in the design and dimensioning of parts. Damage evolution is influenced by interactions between the different constituents of the hybrid, leading to a material behavior that cannot be predicted based on the mechanical properties of the constituents. Detailed knowledge of these interactions and their influence on mechanical behavior is required for efficient application of continuous-discontinuous fiber-reinforced composites.

Within the past few years, several researchers have worked on continuous-discontinuous fiber-reinforced SMC materials in the context of design, manufacturing, simulation and characterization to contribute to a fundamental understanding of these hybrid material systems [1] and study the effects of hybridization on their mechanical properties [4–6]. The definition of the hybridization effect, which was coined by Hayashi [7], originally described the failure strain enhancement of unidirectional carbon fibers when combined with more ductile glass fibers. Generally, a hybridization effect can describe the enhancement of a distinct property of the hybrid with respect to one of the components serving as a reference or a deviation of the property from a rule of mixtures [8]. Trauth and Weidenmann [4] studied the effects of hybridization of SMC composites with a discontinuous glass fiber-reinforced core and continuous carbon fiber-reinforced face plies. They reported an increase of 171 % and 151 % in tensile and compressive moduli of elasticity, respectively, and an increase of 204 % in tensile strength, compared to the baseline discontinuous SMC constituent. Furthermore, Trauth [6] showed that flexural stiffness and

strength of continuous-discontinuous SMC were 370 % and 101 % higher, respectively, compared to discontinuous SMC. Hybridization also had a positive effect on the maximum force and energy in puncture tests [5].

The effects of hybridization may also depend on the loading conditions since distinct damage mechanisms may manifest (e.g., quasi-static or fatigue). Therefore, results obtained under monotonic loading conditions, such as those reported in the previous studies, cannot simply be transferred to the case when cyclic loading is applied. While the fatigue damage behavior of discontinuous glass fiber SMC [10–12], unidirectional carbon fiber-reinforced composites [13–16] and cross-ply laminates [17–19] is largely understood, investigations on the fatigue behavior of continuous-discontinuous fiber-reinforced SMCs were mainly limited to material systems with glass fibers serving both as continuous and discontinuous reinforcement [20–22]. Due to the low difference in failure strain of both components, effects of hybridization were not particularly pronounced and the hybrid composites only showed a moderate resistance to fatigue. To date, no studies have reported the fatigue behavior of hybrid materials consisting of discontinuous glass fiber SMC with continuous carbon fiber reinforcements. To the knowledge of the authors, only two reported studies addressed the fatigue behavior of hybrid composites combining continuous carbon and glass fibers reinforcements [23,24]. Dickson et al. [23] showed, that hybrid composites combining unidirectional glass and carbon fibers in an alternating layer configuration (carbon fiber volume ration of 25 %, 50 % and 75 %) showed a higher fatigue ratio compared to both of the components. The fatigue ratio was defined by the fatigue strength at 10^6 cycles divided by the ultimate tensile strength. Hofer et al. [24] studied quasi-isotropic glass/carbon hybrid composites and found the tensile fatigue behavior to be comparable to that of entirely carbon fiber reinforced composites, when using a carbon to glass ratio of 2:1. The results suggest that reinforcing discontinuous glass fiber SMC with continuous carbon fibers might lead to a material system with promising fatigue properties.

The current study is focused on analyzing the effects of hybridization on the fatigue life and damage evolution of a discontinuous glass fiber-reinforced SMC and continuous carbon fiber material system with an UPPH resin system. Two different material configurations were investigated, which consist of a discontinuous glass fiber SMC core and either unidirectional ([0/DiCo/0]) or cross-ply ([0/90/DiCo/90/0]) carbon fiber-reinforced face plies. The first configuration corresponds to the material system analyzed by Trauth et al. [4–6] under monotonic loading conditions. The second configuration was additionally analyzed, as it is potentially useful for applications subjected to multiaxial loading.

2. Materials and specimen geometries

2.1. Materials and manufacturing

Continuous and discontinuous semi-finished sheets were manufactured on a conveyor plant type HM-LB-800 (Schmidt and Heinzmann) at the Fraunhofer Institute for Chemical Technology, Pfinztal, Germany. An unsaturated polyester-polyurethane hybrid (UPPH) two-step curing resin system [9] served as matrix for both continuous and discontinuous SMC, which allowed for a continuous homogeneous matrix phase in the hybrid continuous-discontinuous fiber-reinforced SMC plaques. The reader is referred to [4] for detailed information on the composition of the resin system itself. To manufacture the discontinuous semi-finished material, the resin was applied to an upper and lower carrier foil. E-glass fiber strands were then chopped to 25.4 mm bundles and dispersed onto the lower foil in random orientation. The nominal fiber volume content was 26 % (nominal fiber weight content: 43 %). The fibers were sandwiched between the two foils and the material went through a calendaring zone before being rolled up and allowed to mature for several days. Continuous carbon fiber semi-finished material with a nominal fiber volume content 53 % (nominal fiber weight content: 64 %) was

manufactured by feeding unidirectional carbon fiber non-crimp fabric instead of chopped glass fibers to the conveyor belt. Heating and cooling sections were installed at the end of the SMC manufacturing line to start the curing process by increasing the temperature to 80 °C and then stop the cross-linking reactions by cooling the material down to room temperature again. The temperature profile was chosen in a way that the first reaction of the two-step curing was completed after this manufacturing step, thereby increasing the viscosity, which allowed for better handling and cutting.

After maturation, the semi-finished material was cut into plies, stacked and compression molded into plaques of 800 mm length and 250 mm width on a hydraulic press (COMPRESS PLUS DCP-G 3600/3200 AS by Dieffenbacher). The temperature of the mold was set to 145 °C. A constant force of 2500 kN was applied during a mold-closing time of 112 s. In this regard, to manufacture discontinuous glass fiber-reinforced SMC plaques, the stack was placed into the rectangular mold with a mold coverage of 50 % to enforce preferential flow during compression molding. The resulting preferential fiber orientation leads to higher mechanical properties in the direction of flow [4]. Continuous carbon fiber-reinforced SMC plaques were manufactured with a mold coverage of 100 %. The compression molding process of the hybrid continuous-discontinuous fiber-reinforced SMC plaques followed the same strategy for each layer, which is depicted in Fig. 1.

Depending on the desired configuration, one or two continuous semi-finished sheets (with a 0° or 0/90° non-crimp fabric serving as reinforcement) were placed into the mold (100 % mold coverage) followed by a stack of discontinuous SMC (50 % mold coverage) and another one or two (0° or 90°/0°) continuous sheets (100 % mold coverage). The cross-sections of the different materials investigated in this study are depicted in Fig. 2.

2.2. Specimen preparation

Tensile test specimens were extracted via water jet cutting from both the charge and the flow region of the plaques and in the flow direction of the discontinuous material. In the evaluation of the data, no distinction was made between charge and flow region specimens, since they show similar mechanical behavior under tensile loading. This has already been pointed out by Trauth and Weidenmann [4]. End tabs made of glass fiber multi-axial fabric and epoxy (PREGNIT GMBE by Krempel GmbH) were bonded to the Co SMC, [0/DiCo/0] and [0/90/DiCo/90/0] specimens using the acrylic adhesive DP810 (3 M) following the recommendations in DIN EN ISO 527-5 [25]. The specimen width was 15 mm, the total length was 170 mm and the clamping length was 100 mm. A similar width was chosen according to DIN EN ISO 527-5 [25] for all material systems for the purpose of comparability even though this standard gives recommendations for unidirectional reinforced composites only. The geometry deviates from recommendations for discontinuously reinforced composites in DIN EN ISO 527-4 [26]. The length was shorter than recommended in both standards, which was chosen to allow the results to be compared with the existing literature [4]. However, Trauth [6] demonstrated that a reduction of the length and width did not lead to a relevant change of mechanical properties of discontinuous SMC. The thickness of each specimen was measured before testing (Table 1). In addition, four each of the [0/DiCo/0] and [0/90/DiCo/90/0] specimens were analyzed to measure the individual ply thicknesses. The average ply thickness was based on ten measurements along the specimen length in the center of a carbon fiber tow (Table 1).

2.3. Microstructure analysis

The microstructure in discontinuous fiber-reinforced SMC is inhomogeneous over the thickness, due to the plug-like flow [27]. The material in the center exhibits little shear and fibers remain to be arranged in straight bundles. In contrast, high shear stresses in the surface layer close to the mold lead to splicing of the bundles and increasing fiber
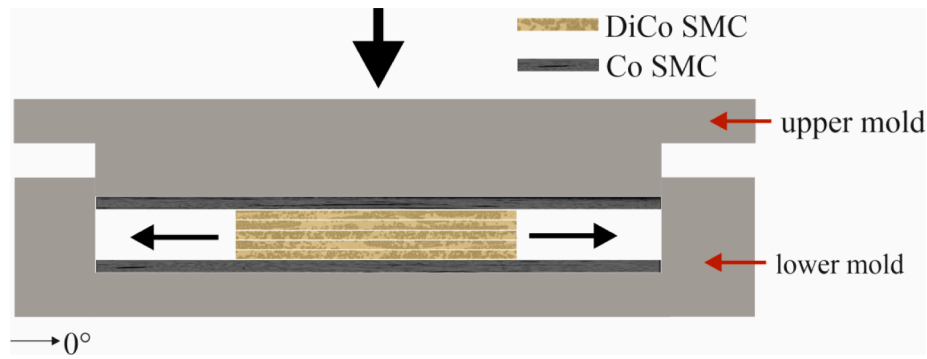
Fig. 1. Schematic illustration of the compression molding process of a [0/DiCo/0] plaque. Continuous semi-finished sheets are placed into the mold with 100 % mold coverage, whereas the discontinuous semi-finished material exhibits preferential flow in 0°-direction, due to a mold coverage of only 50 %. Black arrows indicate the movement of the upper mold and the flow direction of the semi-finished material.
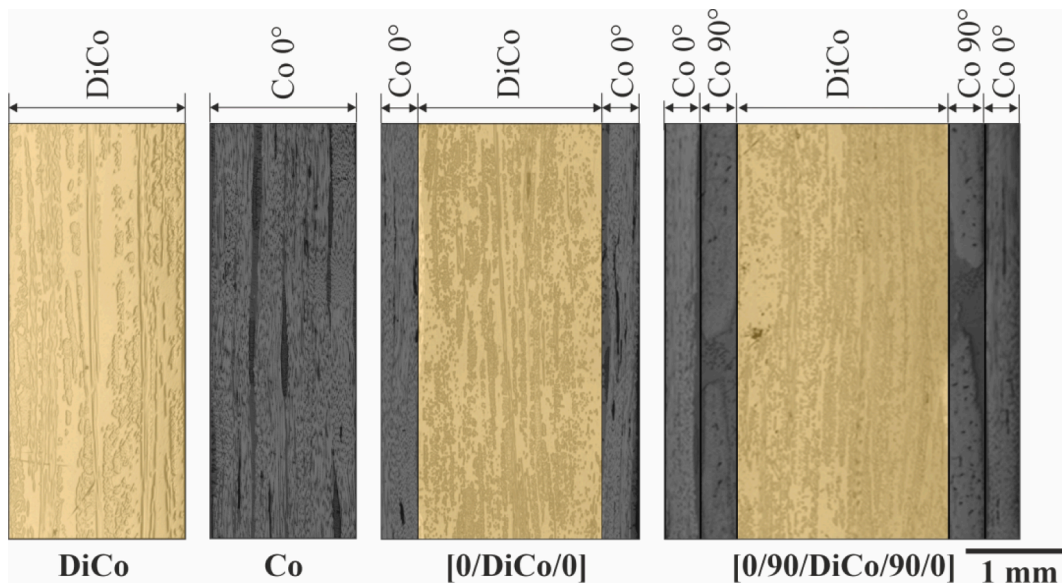

Fig. 2. Schematic representation of the cross-sections of the material systems examined.

Table 1
Average specimen and ply thickness.

	$h_{Specimen}$ (mm)	h_{DiCo} (mm)	h_{Co} (mm)
Co SMC	1.44 ± 0.027	–	–
DiCo SMC	1.74 ± 0.076	–	–
[0/DiCo/0]	2.89 ± 0.077	2.13 ± 0.084	0.32 ± 0.021
[0/90/DiCo/90/0]	3.53 ± 0.120	1.96 ± 0.084	0.32 ± 0.028

curvature. As pointed out by Trauth [4], this effect is higher at the interface region of a continuous and discontinuous ply of hybrid SMC than in the surface layer of solely discontinuous reinforced specimens near the mold. Microstructural investigations carried out in this study showed an increasing amount of bundle splicing and curvature with increasing number of continuous carbon fiber plies. Fig. 3a depicts a sectional view on the center plane (relative to the thickness direction) of five specimens extracted from different positions on [0/90/DiCo/90/0] plaques, which are depicted in Fig. 3b. Moving from left to right (from the charge region to the flow region), the amount of spliced fiber bundles and fiber curvature increases. The characteristic microstructure of discontinuous SMC is observed only within a small area in the center of the plaque thickness. In the flow region, no intact bundle structure remained throughout the whole thickness of the discontinuous ply.

3. Experimental methods

Monotonic tensile tests at quasi-static and fatigue strain rates and tension-tension fatigue tests were carried out according to ISO 13003 [28] and DIN EN ISO 527-1 [29], respectively, on a Zwick Roell 1478 servo-hydraulic testing machine (modified with an additional servo cylinder). The machine was equipped with a load cell (type 1220AJ by Interfaceforce) with a capacity of 100 kN. The ambient test temperature was 21 °C. Specimens were hydraulically clamped with a clamping distance of 100 mm. A capacitor, which measured the displacement of the flange of the actuator was used for displacement control during tensile tests. The quasi-static strain rate was $2\bullet10^{-4}$ s^{-1} and the fatigue strain rate was approximately $2\bullet10^{-1}$ s^{-1}. Since strain was not measured directly on the specimens during the tests at fatigue strain rate, the specified value was approximated based on the failure strain of the materials and the test duration (0.1 s according to ISO 13003 [28]). Tension-tension tests (R = 0.1) were carried out under load control with a frequency of 5 Hz. An infrared camera was used to ensure that cyclic loading resulted in a temperature increase of less than 10 °C. An axial clip-on extensometer (type EXA 50-5) by Sandner Messtechnik GmbH with a gauge length of 50 mm, a measuring displacement of ±5 mm and a measuring error of ±0.2 % was used for strain measurement. The sampling rate of the extensometer was 1000 Hz. The cycle-dependent dynamic stiffness $E_{dyn}(N)$ was determined from the stress–strain
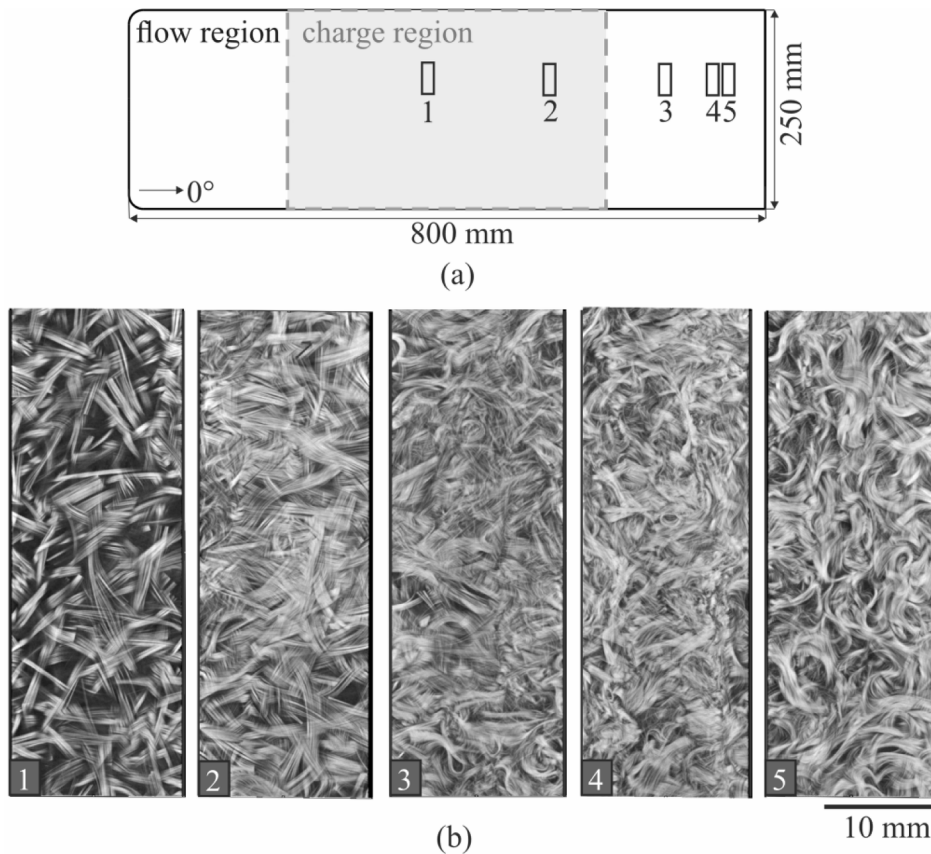
Fig. 3. (a) Position of five specimens extracted from a [0/90/DiCo/90/0] plaque for microstructural investigations and (b) sectional view on the specimens' microstructure obtained from CT scans. Images were taken from the center plane with regard to the thickness direction.

response of the specimens. $E_{dyn}(N)$ corresponds to the secant modulus of the N-th hysteresis loop. Based on the dynamic stiffness, a damage variable was defined by:

$$D(N) = 1 - \frac{E_{dyn}(N)}{E_{dyn,4}}, \qquad (4.1)$$

which presents a measure for the stiffness degradation. The initial dynamic stiffness $E_{dyn,4}$ was determined within the fourth loading cycle, to exclude influences of the start-up behavior of the testing machine.

The maximum number of cycles investigated was $2.6 \cdot 10^6$ cycles. Specimens that did not fail within the investigated cycle range were declared runouts. Failure was defined by separation of the specimen.

In addition to the continuous tests, interrupted tension–tension fatigue tests were carried out with DiCo SMC, [0/DiCo/0] and [0/90/DiCo/90/0] specimens to further analyze damage evolution during cyclic loading. For this purpose, the edges of the specimens were sanded and polished prior to testing to ensure that the microstructure was clearly visible under an optical microscope. The tests were interrupted in steps of one decade of cycles (i.e., 10 cycles, 100 cycles, 1000 cycles, etc.) to inspect the test specimen edges. During each interruption, specimens were unclamped for microscopic investigations and then re-clamped to subject them to further cyclic loading up until the next scheduled interruption. This procedure was repeated until final failure of the specimens. Microscopic images were taken from both specimen edges before testing and after each load step to analyze the weighted crack length in the DiCo ply. According to Quaresimin et al. [30], the weighted crack was defined by:

$$\rho_w = \frac{\sum_{i=1}^{n} L_{c,i}}{L_G h_{DiCo}}, \qquad (3.1)$$

with the total number of cracks n, the length of the i-th crack $L_{c,i}$, the gauge length L_G, and the thickness of the discontinuously reinforced ply h_{DiCo}.

4. Results

4.1. Monotonic tensile tests

Results of the tensile tests at quasi-static and fatigue strain rates are given in Table 2. Tensile strength was strain rate-dependent for all investigated materials, with DiCo SMC showing the most pronounced strain rate-dependence.

4.2. Tension-tension fatigue tests

4.2.1. S-N data
Fig. 4 depicts the stress-life data of all tested specimens. The fatigue strength of DiCo SMC decreased by approximately 10 % UTS^F per

Table 2
Ultimate tensile strength at quasi-static (UTS^S) and fatigue strain rate (UTS^F). $\bar{x}$ represents the mean value of five specimens, μ is the standard deviation and CV the coefficient of variation.

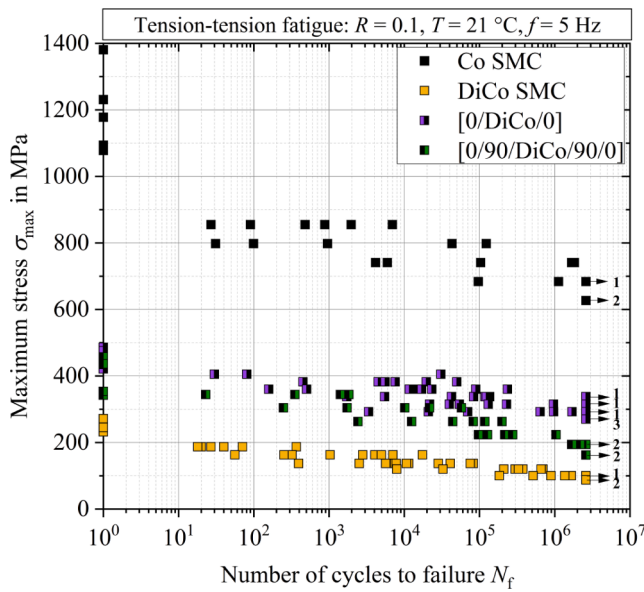|	UTS^S			UTS^F		
	$\bar{x}$ (MPa)	μ (MPa)	CV (%)	$\bar{x}$ (MPa)	μ (MPa)	CV (%)
Co	1002	142.2	14.2	1140	168.8	14.8
DiCo	197	15.0	7.6	237	14.5	5.9
[0/DiCo/0]	445	22.0	4.9	456	26.5	5.8
[0/90/DiCo/90/0]	382	23.2	6.1	405	52.9	13.1

Fig. 4. S-N data of the material systems examined in this study. Results from tensile tests at fatigue strain rate are depicted on the y-axis. Runouts are marked with arrows. The number behind the arrows indicate the corresponding number of runout specimens.

decade of cycles, which is typical for conventional SMC composites [11,31,32]. The fatigue ratio, which in this study was defined as the stress at which all specimens were declared runouts divided by UTS^F, was 0.37 for the DiCo SMC and 0.55 for the Co SMC. [0/DiCo/0] specimens exhibited a fatigue ratio of 0.6, which was greater than both of its constituents, and single runouts at stresses as high as 75 % UTS^F. The maximum stress at which all tested [0/DiCo/0] specimens were runouts was 209 % higher than the maximum stress at which all tested DiCo SMC specimens were runouts. In contrast UTS^F of [0/DiCo/0] specimens was only 92 % higher than UTS^F of DiCo SMC. The fatigue ratio of [0/90/DiCo/90/0] specimens was 0.4, which was comparable to DiCo SMC. The maximum stress at which all [0/90/DiCo/90/0] specimens were runouts was 86 % higher than the maximum stress at which all tested DiCo SMC specimens were runouts, whereas UTS^F increased by 71 % compared to DiCo SMC.

Since the predominant mechanisms leading to failure of a composite are effective only in a limited range of applied maximum strain [13], there is merit for expressing fatigue-life data in terms of strain instead of stress, to better evaluate hybridization effect. For this purpose, maximum stresses were converted to initial maximum strains by using the average initial dynamic stiffness given in Table 3.

The resulting strain-life diagrams are depicted in Fig. 5. The solid lines represent S-N curves, which were approximated by using the restricted form of the power law function $\log(\varepsilon) = A - B\log(N)$. The parameters A and B were obtained via linear regression. While [0/DiCo/0] specimens showed a behavior similar to that of Co SMC under monotonic loading, cyclic loading at an initial maximum strain of 1.1 % resulted in a behavior similar to that of DiCo SMC. At high numbers of cycles ($>5\cdot10^5$), initial maximum strain values of [0/DiCo/0] specimens were above those of Co and DiCo SMC.

Table 3
Average initial dynamic stiffness of all examined materials including the respective standard deviation.

	Co SMC	DiCo SMC	[0/DiCo/0]	[0/90/DiCo/90/0]
$\overline{E}_{dyn,4}$ (GPa)	103.9 (μ = 2.1)	13.9 (μ = 0.8)	36.48 (μ = 1.9)	30.19 (μ = 1.0)

In contrast, [0/90/DiCo/90/0] specimens showed higher fatigue strains under monotonic loading compared to [0/DiCo/0] specimens. However, the performance under cyclic loading decreased significantly. Initial maximum strain values at $2.6\cdot10^6$ cycles ranged within those of Co and DiCo SMC.

4.2.2. Post-mortem damage analysis

The main damage mechanisms observed in [0/DiCo/0] specimens under cyclic loading were similar to those observed under monotonic loading, but differed in terms of their number and the sequence of their occurrence. The specimens showed splitting cracks and fiber fracture in the Co plies, delamination between the DiCo and Co plies, as well as matrix cracks and fiber bundle pull-out in the DiCo ply (Fig. 6). The density of splitting cracks was higher in specimens tested under cyclic load than in those tested monotonically. The crack density in the DiCo ply was also higher across the entire specimen length than in monotonically loaded specimens. The proportion of different damage mechanisms was very distinct from specimen to specimen.

Runout specimens showed almost no signs of damage in the Co plies except detached stitching fibers and some splitting cracks at the specimen edges, whereas a large amount of matrix cracks over the entire specimen length and local formation of crack networks were observed in the DiCo ply (Fig. 7). These matrix cracks are difficult to see on unpolished specimens with the naked eye but can be identified by the local whitish discoloration of the DiCo ply.

The damage pattern of [0/90/DiCo/90/0] specimens was dependent on the maximum stress. Fig. 8 shows a specimen that was tested at 75 % UTS^F showing large scale delamination of the 0° carbon fiber plies, whereas the interface between the 90° ply and the DiCo ply remained largely intact. Fiber fracture occurred at different positions across the entire specimen length. The density of splitting cracks was higher than in monotonically loaded specimens. Several matrix cracks could be observed across the specimen length, but the crack density was lower compared to [0/DiCo/0] specimens.

For specimens tested at lower maximum stresses, damage was more localized. The specimen depicted in Fig. 9 was tested at 55 % UTS^F. Fiber fracture, splitting cracks and delamination between the 0° and the 90° plies occurred in the region of final failure. In contrast, only few splitting cracks were observed across the rest of the specimen length together with partial delamination of a misaligned 0° carbon fiber tows at the specimen edge. In the DiCo ply, hardly any matrix cracks were observed apart from the site of ultimate failure.

4.2.3. Damage evolution

The damage variables of representative Co SMC, DiCo SMC, [0/DiCo/0] and [0/90/DiCo/90/0] specimens, which were tested at different maximum stresses, are depicted in Fig. 10. DiCo SMC specimens showed a common trend with a high initial increase within the first 5 % of fatigue life, a damage parameter D of 0.1 after 50 % of fatigue life, and $D > 0.13$ before final failure. Only the specimen tested at 79 % UTS^F showed a deviant behavior. The curved obtained for Co SMC were less smooth due to several jumps that resulted from fiber cluster fracture. In general, D increased more gradually compared to DiCo SMC and was below 0.5 after 50 % of fatigue life. Due to the stochastic nature of the fiber cluster breaks, the values of D deviated strongly before final failure. For [0/DiCo/0] specimens, the initial increase of D was less pronounced than for DiCo SMC and its value after 50 % of fatigue life was approximately half the value obtained for DiCo SMC. For [0/90/DiCo/90/0] specimens, higher cross-specimen variations were observed but the behavior was generally comparable to that of DiCo SMC.

Microscopic investigation carried out within interrupted fatigue tests revealed, that damage evolution in the DiCo ply of [0/DiCo/0] specimens was similar to that usually observed in solely discontinuously reinforced SMC [11]. Matrix cracks predominantly oriented normal to the loading direction were the main damage mechanism responsible for stiffness degradation. The number of matrix cracks increased with
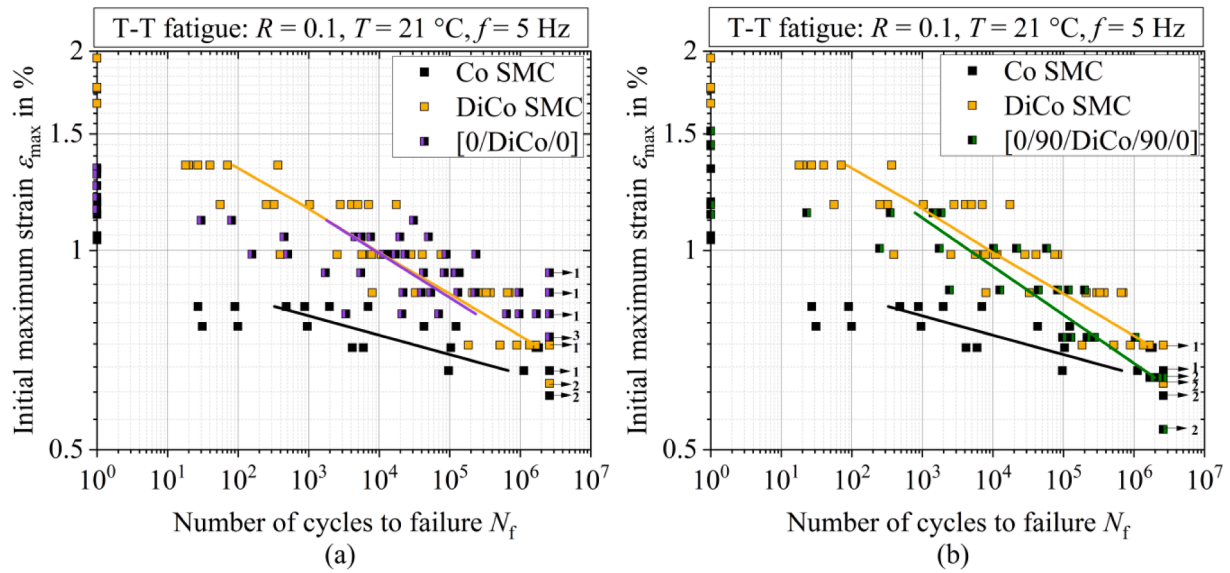
Fig. 5. Strain-life data of (a) [0/DiCo/0] and (b) [0/90/DiCo/90/0] specimens including strain-life data of Co and DiCo SMC for comparison. Initial maximum strains were calculated by using the initial dynamic stiffness of the corresponding specimens. Solid lines depict strain-life curves obtained via linear regression.
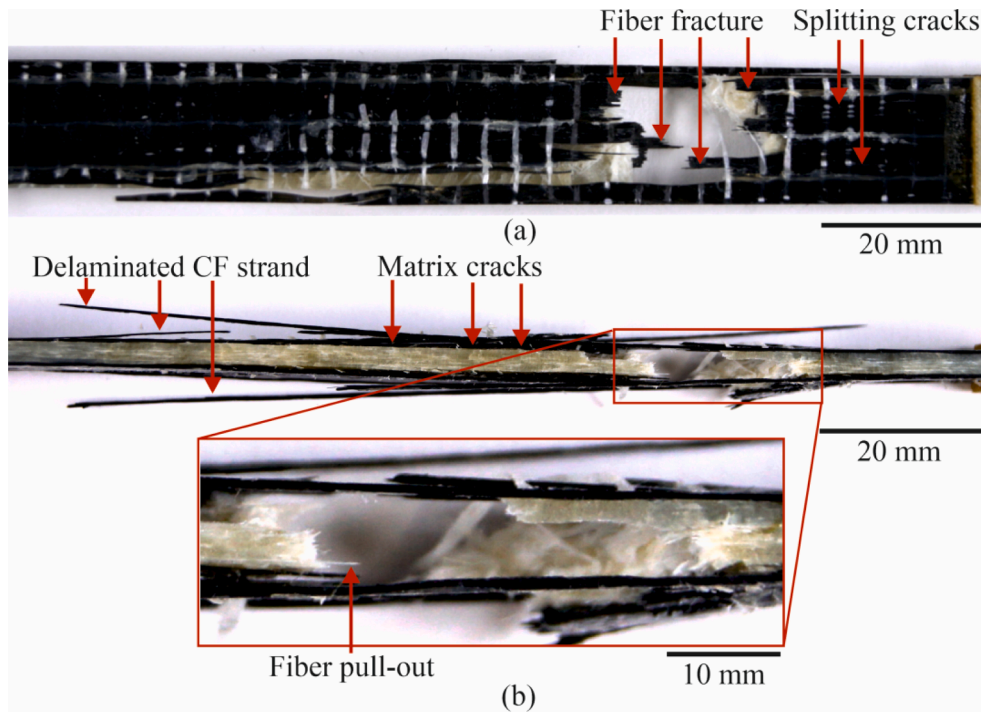

Fig. 6. (a) Top view and (b) side view of a [0/DiCo/0] specimen that was tested at 85 % UTS[F].

increasing numbers of cycles, which is depicted in Fig. 11. Fiber fracture occurred locally at the specimen edges at an early stage of fatigue life ($N = 10^2$) and initiated delamination ($N = 10^3$). A pronounced stiffness reduction between 10^4 and 10^5 cycle occurred due to coalescence of cracks and pseudo-delamination, marked by red arrows, observed in the lower right panel of Fig. 11, prior to final failure, which occurred outside the gauge length.

The microscopic investigation further showed that the weighted crack length in DiCo SMC increased with the number of cycles in the same manner as stiffness decreased. Evolution of weighted crack length in the DiCo ply of [0/DiCo/0] specimens was largely unaffected by the continuous reinforcement. Fig. 12 shows the absolute stiffness loss and the weighted crack length of three different DiCo specimens tested at 51 % and

58 % UTS[F] as well as one [0/DiCo/0] specimen tested at 75 % UTS[F]. After around 10^{-1} of total fatigue life, the stiffness loss of the [0/DiCo/0] specimen deviates from the curves obtained for DiCo SMC specimens, due to fracture and delamination of the continuous carbon fiber plies.

In [0/90/DiCo/90/0] specimens, a large amount of ply cracks formed in the 90° ply after only 10 cycles (Fig. 13). These cracks grew into the DiCo ply with additional loading and initiated delamination between the 0° and the 90° continuous plies. Coalescence of these propagating ply cracks led to separation of the specimen. The number of matrix cracks that formed within the DiCo ply independently of the 90° ply cracks was negligible compared to the crack density that was observed in DiCo and [0/DiCo/0] specimens. Fig. 14 shows the absolute stiffness loss and the weighted crack length of the [0/90/DiCo/90/0]
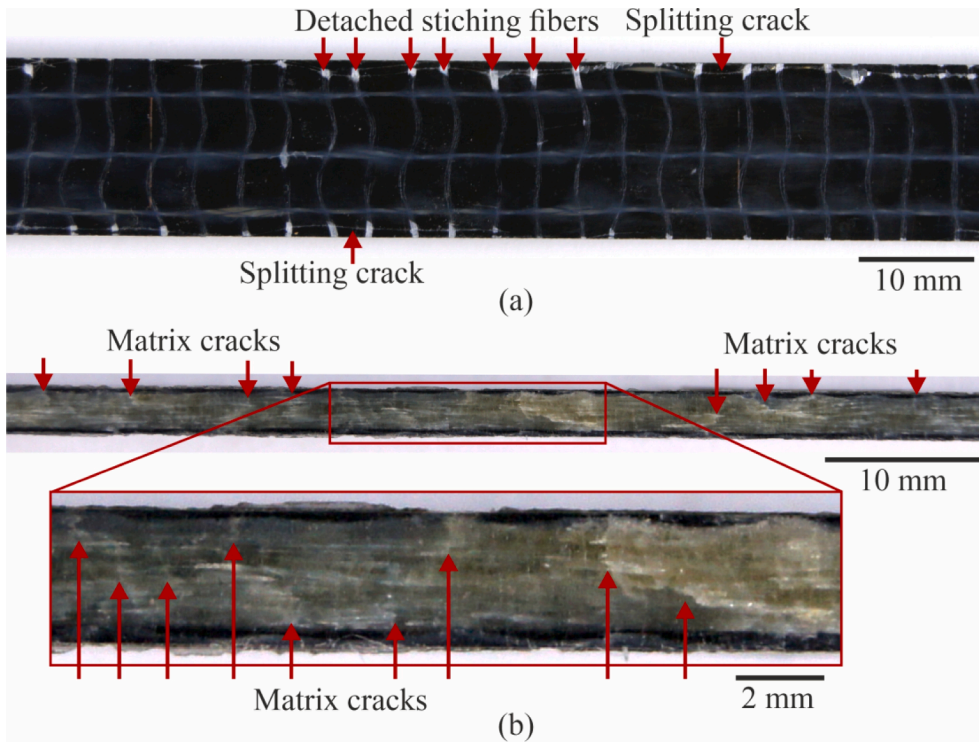
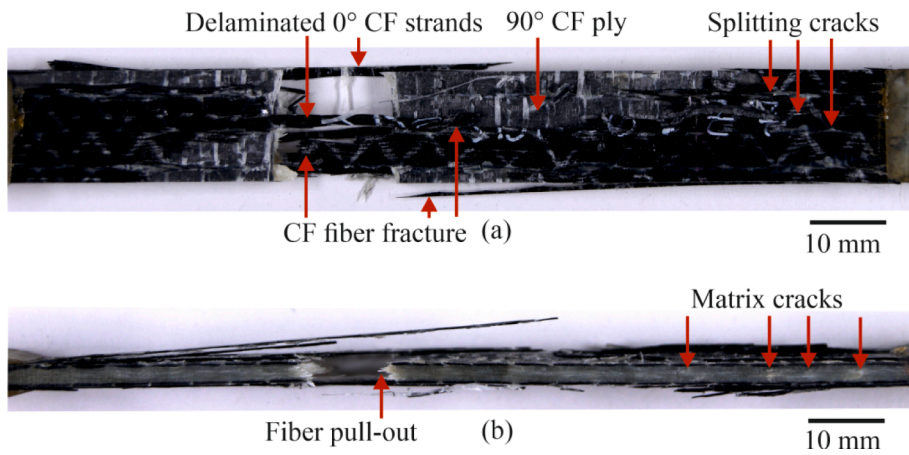**Fig. 7.** (a) Top view and (b) side view of a [0/DiCo/0] specimen (runout) that was tested at 60 % UTS^{F}.

Fig. 8. (a) Top view and (b) side view of a [0/90/DiCo/90/0] specimen that was tested at 75 % UTS^{F}.
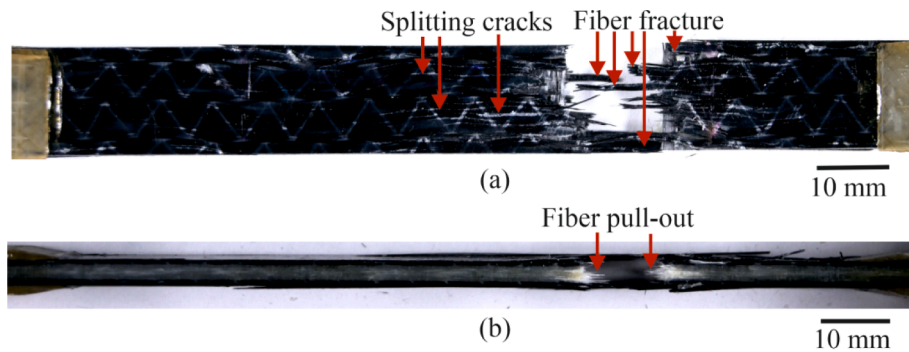

Fig. 9. (a) Top view and (b) side view of a [0/90/DiCo/90/0] specimen that was tested at 55 % UTS^{F}.
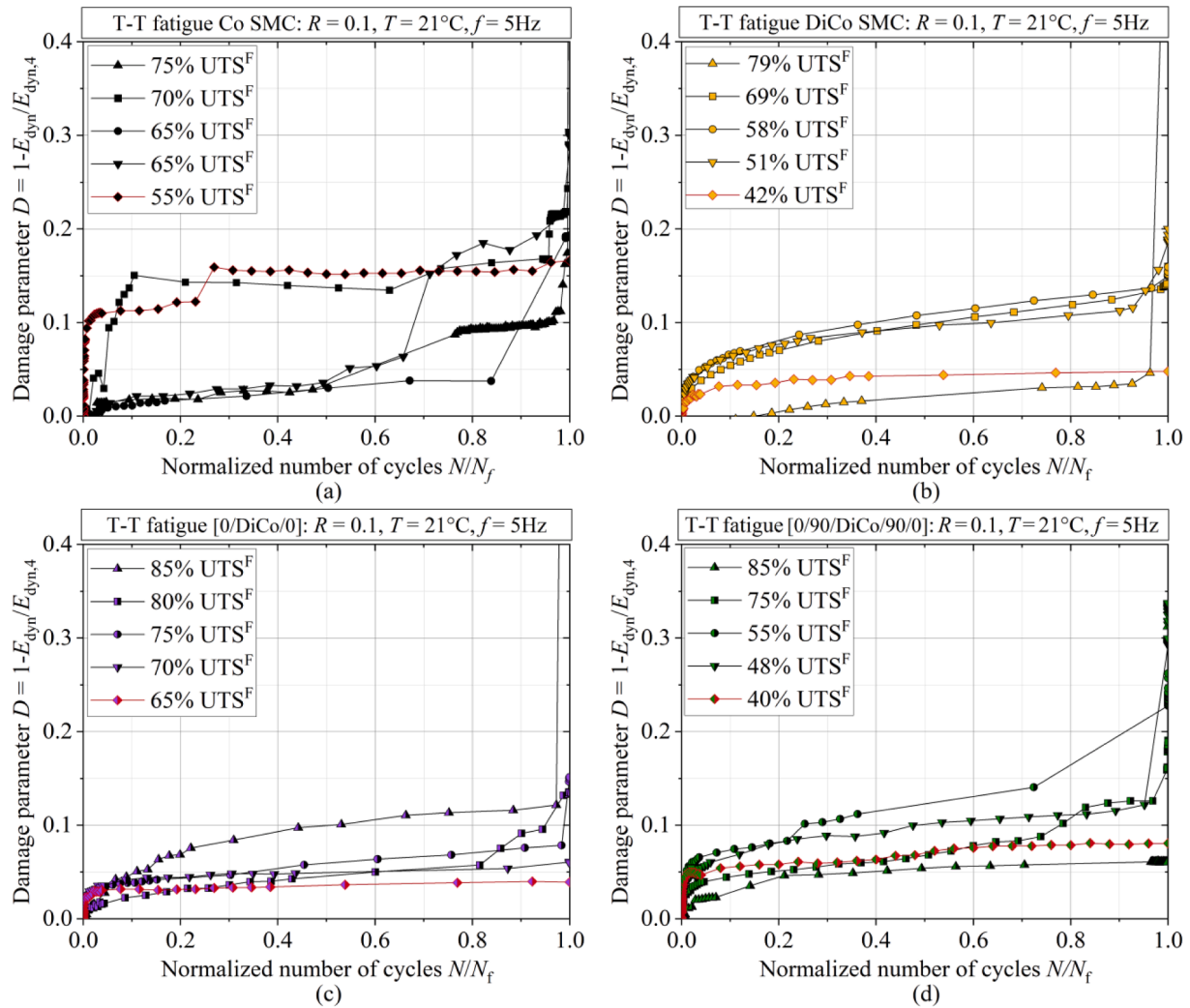
Fig. 10. Damage variable of representative (a) Co SMC, (b) DiCo SMC, (c) [0/DiCo/0] and (d) [0/90/DiCo/90/0] specimens tested at different stresses. Data outlined in red represent runouts, for which N_f was replaced by $2.6 \cdot 10^6$ cycles. (For interpretation of the references to colour in this figure legend, the reader is referred to the web version of this article.)

specimen tested at 65 % UTS^F compared to the results obtained from the three different DiCo SMC specimens tested at 51 % and 58 % UTS^F, that have already been shown in Fig. 12.

5. Discussion

5.1. [0/DiCo/0] specimens

Under monotonic loading, the damage behavior of [0/DiCo/0] specimens was clearly dominated by the Co plies, which failed first, resulting in additional stresses in the DiCo ply that ultimately exceeded its ultimate strength. Trauth and Weidenmann [4], who studied the same material system, observed a similar failure behavior. In contrast, mechanical behavior and damage evolution of [0/DiCo/0] specimens were dominated by the DiCo ply under cyclic loading, especially in the high cycle fatigue range. Below 1.1 % initial maximum strain ($>10^3$ cycles), the strain-life curve of [0/DiCo/0] specimens matched the corresponding curve of DiCo SMC specimens almost exactly (Fig. 5a). This means that the Co plies were subjected to strains that exceeded the failure strain of non-hybrid Co SMC specimens. At high numbers of cycles ($>5 \cdot 10^5$), [0/DiCo/0] specimens performed even better than both Co and DiCo SMC specimens with regards to fatigue ratio and initial maximum strain. While all examined [0/DiCo/0] specimens tested at 0.74 % initial maximum strain were runout, all Co SMC specimens and

almost all DiCo SMC specimens failed below $2.6 \cdot 10^6$ cycles due to fatigue. Similar conclusions resulted from an analysis of the damage behavior of [0/DiCo/0] specimens. Under monotonic loading, the Co plies failed first, whereas runout specimens were characterized by a large amount of matrix cracks in the DiCo ply and almost no signs of damage in the Co plies. The continuous reinforcement even supported the DiCo ply by bridging regions where matrix cracks formed networks, which would have otherwise led to final failure without the additional support.

Enhancement of failure strain of the Co plies is assumed to have two main causes: (*i*) residual stresses, and (*ii*) a change in the damage evolution. Residual stresses originate from thermal cool down after curing during the compression molding process. Due to the mismatch in thermal expansion coefficients between the DiCo and Co plies, mechanical strains $\Delta\varepsilon_{Co}$ and $\Delta\varepsilon_{DiCo}$ generate in the plies that can be approximated by:

$$\varepsilon(\Delta T) = \alpha_{Co}\Delta T + \Delta\varepsilon_{Co} = \alpha_{DiCo}\Delta T + \Delta\varepsilon_{DiCo}. \tag{5.1}$$

The coefficient of thermal expansion of Co SMC was approximated by:

$$\alpha_{Co} = \frac{E_{CF}\alpha_{CF}\gamma_{CF} + E_{UPPH}\alpha_{UPPH}(1 - \gamma_{CF})}{E_{CF}\gamma_{CF} + E_{UPPH}(1 - \gamma_{CF})}, \tag{5.1}$$
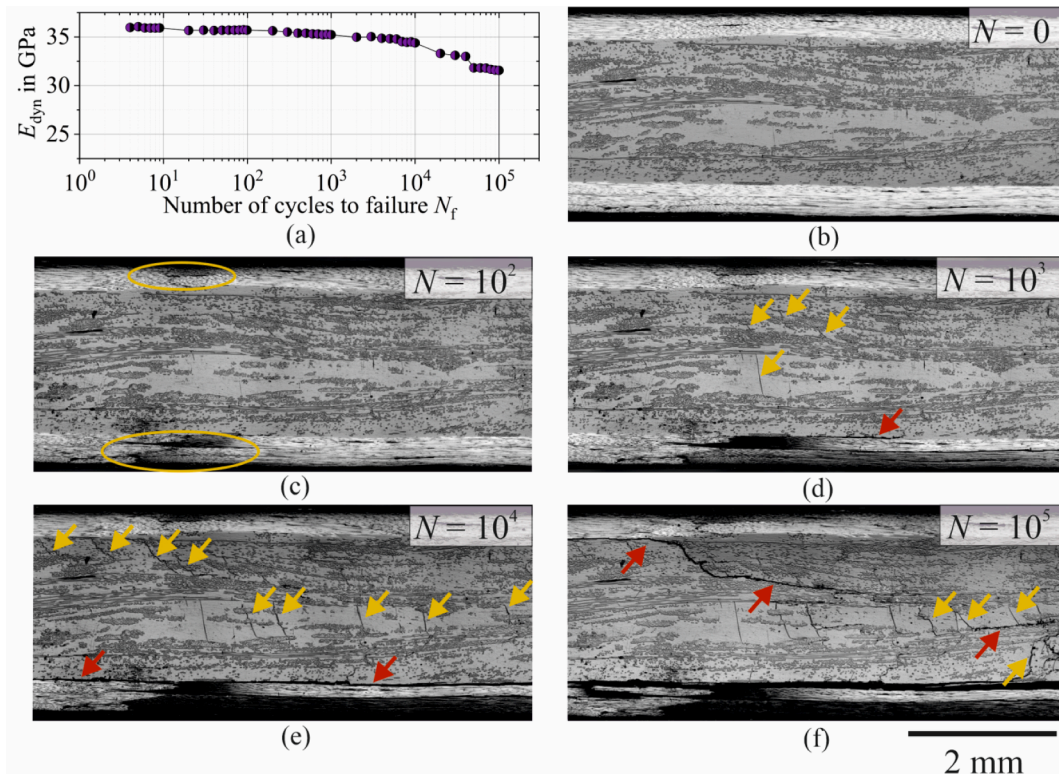
Fig. 11. (a) Stiffness degradation curve and (b)-(f) edge section of a [0/DiCo/0] specimen tested at 75 % UTS^F after different numbers of cycles. Yellow arrows indicate matrix cracks, whereas red arrows indicate delamination between the Co and DiCo ply or pseudo-delamination within the DiCo ply. Ellipses in (c) mark regions of fiber fracture. (For interpretation of the references to colour in this figure legend, the reader is referred to the web version of this article.)
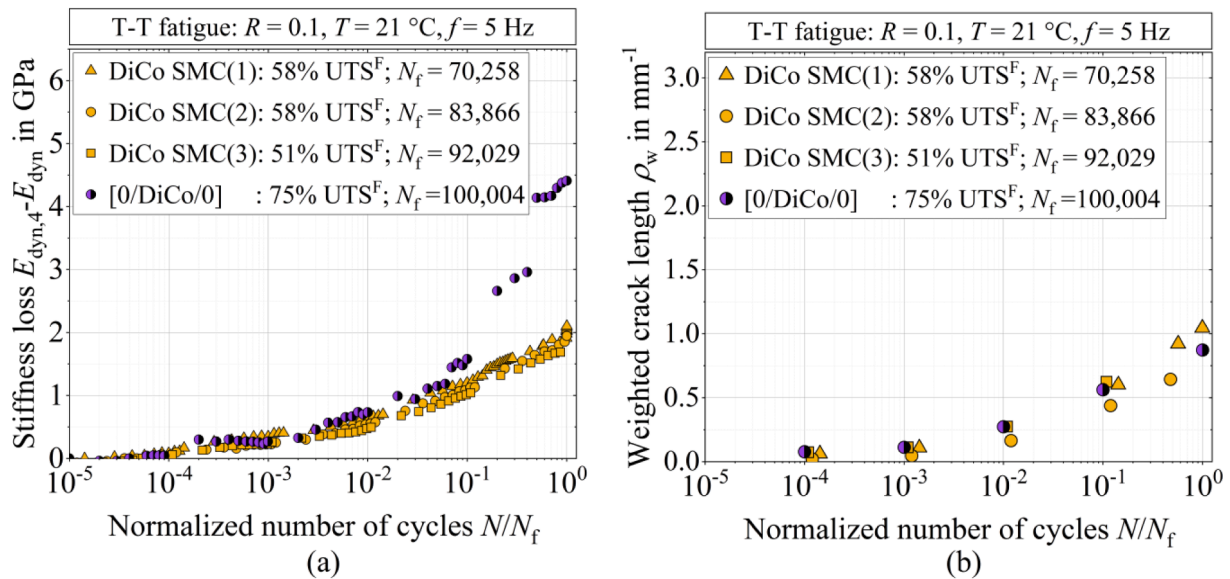

Fig. 12. (a) Stiffness loss and (b) weighted crack length of three DiCo SMC specimens and a [0/DiCo/0] specimen, that failed after similar numbers of cycles.

with the Young's modulus of the carbon fibers $E_{CF} = 242$ GPa [33] and the UPPH resin system $E_{UPPH} = 3.45$ GPa [6], the carbon fiber volume content $\gamma_{CF} = 0.64$ (cf. Section 2) and the coefficient of thermal expansion of the carbon fibers $\alpha_{CF} = 8 \cdot 10^{-8}$ K^{-1} [34]. The coefficient of thermal expansion of DiCo SMC $\alpha_{DiCo} = 1.6 \cdot 10^{-5}$ K^{-1} and the UPPH resin system $\alpha_{UPPH} = 6.1 \cdot 10^{-5}$ K^{-1} were determined in a dilatometer test at the Institute of Engineering Mechanics, Karlsruhe Institute of Technology. The temperature difference $\Delta T = -124$ K resulted from cooling down the plaques to room temperature after compression molding at

145 °C. Residual stresses must lead in an equilibrium of forces, which simplified, by applying Hooke's law, yields to:

$$E_{Co}\gamma_{Co}\Delta\varepsilon_{Co} = -E_{DiCo}\gamma_{DiCo}\Delta\varepsilon_{DiCo}. \tag{5.2}$$

γ_{Co} and γ_{DiCo} represent the volume fractions of the Co plies and the DiCo ply, respectively, and were determined by using the ply thicknesses given in Table 1. By inserting Equation (5.1), the initial strain in the Co plies can be calculated by:
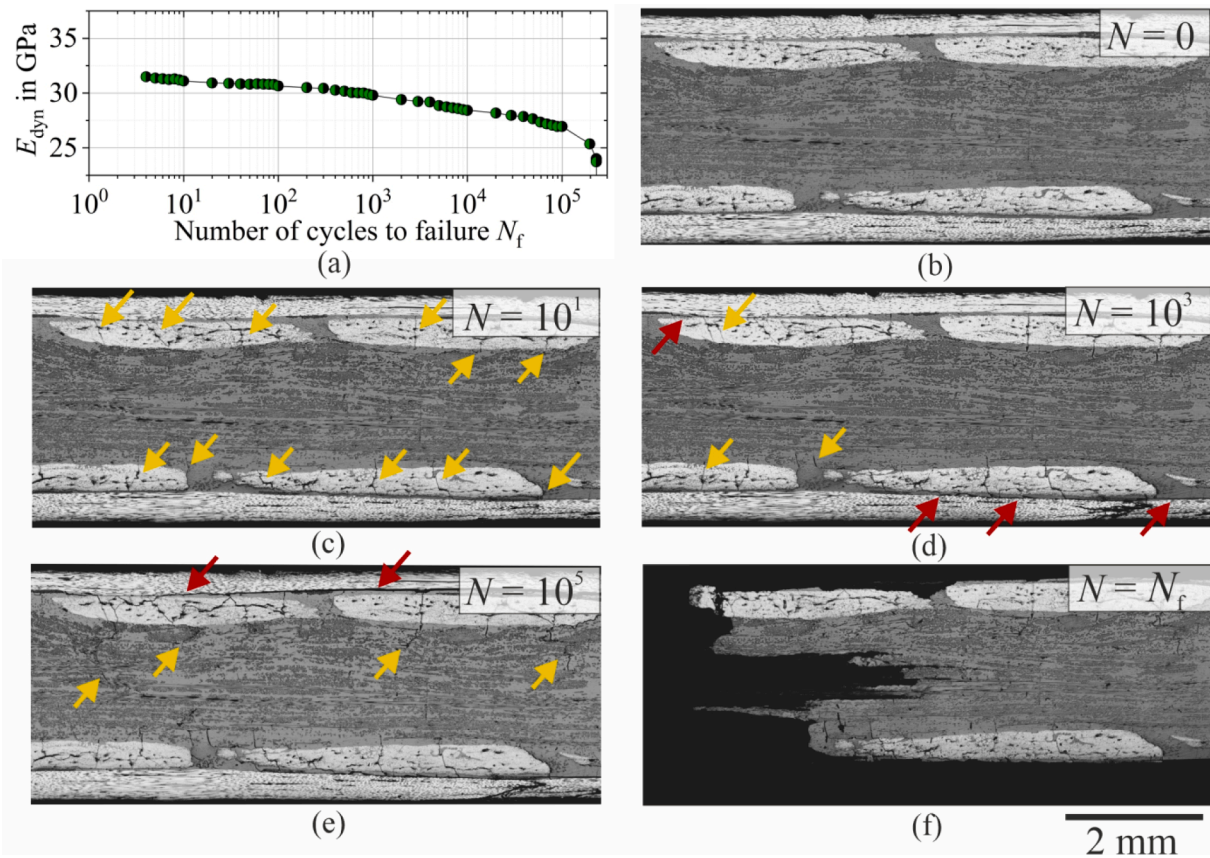
Fig. 13. (a) Stiffness degradation curve and (b)-(f) edge section of a [0/90/DiCo/90/0] specimen tested at 55 % UTS^F after different numbers of cycles. Yellow arrows indicate matrix cracks, whereas red arrows indicate delamination. (For interpretation of the references to colour in this figure legend, the reader is referred to the web version of this article.)
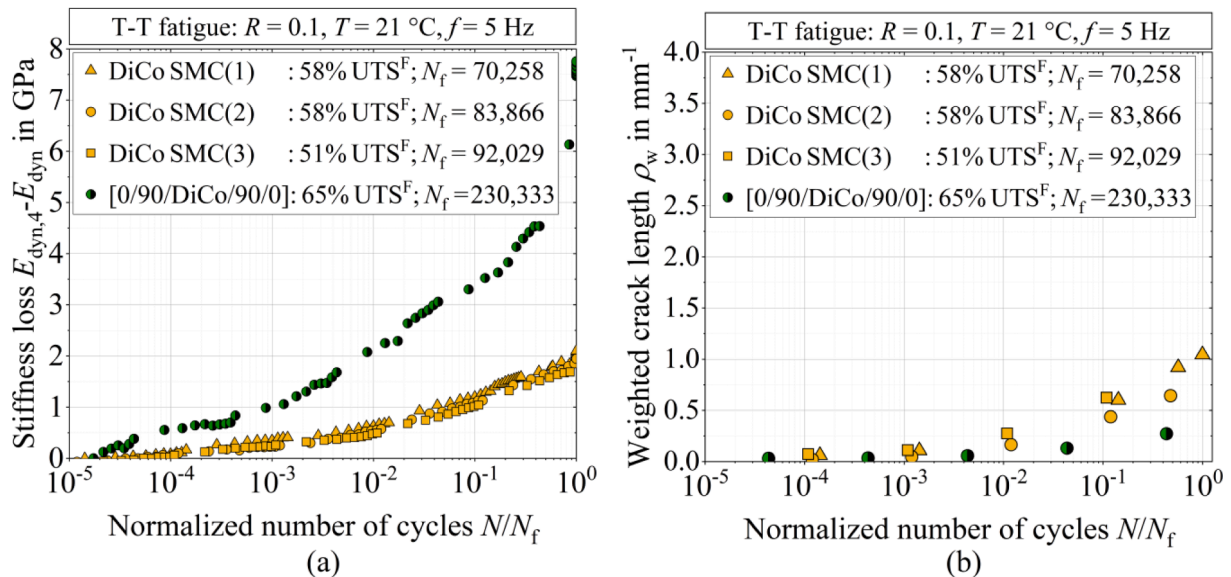

Fig. 14. (a) Stiffness loss and (b) weighted crack length of three DiCo SMC specimens and a [0/90/DiCo/90/0] specimen.

$$\Delta\varepsilon_{Co} = \frac{E_{dyn,4,DiCo}\gamma_{DiCo}}{E_{dyn,4,DiCo}\gamma_{DiCo} + E_{dyn,4,Co}\gamma_{Co}}\alpha_{DiCo}\Delta T, \tag{5.3}$$

in which E_{Co} and E_{DiCo} have been replaced by the initial dynamic stiffness $\overline{E}_{dyn,4,Co}$ and $\overline{E}_{dyn,4,DiCo}$, since those values could be measured during the fatigue tests. Due to an almost linear stress–strain behavior of the

examined materials, this assumption was found to be reasonable.

Equation (5.3) yields $\Delta\varepsilon_{Co} = 0.059\%$, which is well below the strain enhancement depicted in Fig. 5a. Therefore, the higher exploitation of the carbon fibers' mechanical performance must be mainly attributed to the altered damage evolution. In accordance to the hybridization effects described by Swolfs et al. [8], the comparatively ductile DiCo plies

bridged local fiber fracture of the more brittle Co SMC plies, reduced stress concentrations, which led to delayed occurrence of fracture in adjacent fibers and increased the critical size of fiber fracture clusters.

The observations discussed allow a rough estimation of the fatigue behavior of [0/DiCo/0] specimens based on the properties of the components by using an empirical modeling approach. Knowing that the fatigue behavior of [0/DiCo/0] specimens is largely dominated by the DiCo ply justifies the following assumption:

A stress applied to the hybrid material equals the fatigue strength of the hybrid at a specific number of cycles N, if it results in a stress in the DiCo ply, which equals the fatigue strength of DiCo SMC at the same number of cycles N.

Under the assumption of equal strains in all plies, a linear elastic material behavior of all plies and a plane stress condition as well as neglecting the Poissons' effect, Hooke's law provides:

$$\sigma_{\mathrm{Co}} = \frac{E_{\mathrm{Co}}}{E_{\mathrm{DiCo}}} \sigma_{\mathrm{DiCo}.} \tag{5.4}$$

With Equation (5.4) the homogenized stress of a [0/DiCo/0] specimen can be calculated by:

$$\sigma_{[0/\mathrm{DiCo}/0]}(N) = \sigma_{\mathrm{DiCo}}(N)\left(\gamma_{\mathrm{DiCo}} + \frac{E_{\mathrm{dyn,4,Co}}}{E_{\mathrm{dyn,4DiCo}}}\gamma_{\mathrm{Co}}\right). \tag{5.5}$$

Herein σ_{Co}, σ_{DiCo} and $\sigma_{[0/\mathrm{DiCo}/0]}$ represent fatigue stresses and are functions of the number of cycles N. The tensile moduli of elasticity have been replaced by the initial dynamic stiffness for reasons already discussed.

The S-N curve of [0/DiCo/0] specimens can be approximated by using Equation (5.5), with $\sigma_{\mathrm{DiCo}}(N)$ representing the S-N curve of DiCo SMC. The result is shown in Fig. 15. The solid yellow line depicts the analytically determined S-N curve based on the empirical model described herein, while the solid purple curve depicts the experimental results. Model and experiment show good correlation for medium numbers of cycles. The model overestimates the fatigue life of [0/DiCo/0] specimens in the low cycle fatigue range. Here, fatigue life is rather limited by its ultimate fatigue strength under monotonic loading, which

is dominated by the Co plies. For high numbers of cycles ($>5 \cdot 10^5$ cycles), the model underestimated the fatigue strength of [0/DiCo/0] specimens and hence presents a conservative estimate. Additionally, P-S-N curves with a failure probability of $P_S = 10\%$ and $P_S = 90\%$ were determined for both DiCo SMC and [0/DiCo/0] specimens to display the scatter range of the data. Analytical P-S-N curves of [0/DiCo/0] specimens were obtained by inserting the P-S-N curves of DiCo SMC specimens in Equation 5.2. Since scatter was more pronounced in [0/DiCo/0] compared to DiCo SMC specimens, the analytically determined P-S-N curves are closer together than the experimentally determined ones. In the case of DiCo SMC, scatter is mainly attributed to different fiber volume contents and fiber orientation distributions both across plaques and at different positions within a plaque [6,35]. For [0/DiCo/0] specimens, additional variations in fiber volume content in the Co plies, fiber misalignment, and undulations lead to even larger microstructural differences and thus increased scatter.

Fig. 10 showed that stiffness degradation of [0/DiCo/0] specimens was less pronounced than that of DiCo SMC specimens. The Co plies supported the DiCo ply, as long as they were not overloaded. Therefore, if a fatigue criterion was defined by a critical amount of stiffness degradation instead of ultimate failure, the performance of [0/DiCo/0] compared to DiCo SMC specimens is further enhanced.

5.2. [0/90/DiCo/90/0] specimens

In comparison with [0/DiCo/0] specimens, [0/90/DiCo/90/0] specimens showed a less pronounced Co SMC-dominated behavior under monotonic loading (cf. Fig. 5b). Under cyclic loading, the initial maximum strain was significantly higher compared to Co SMC but still below that of DiCo SMC. Runouts were obtained for initial maximum strains similar to those of DiCo SMC and Co SMC. Hence, no effect of hybridization in terms of initial maximum strain was observed for [0/90/DiCo/90/0] specimens. Comparatively low stresses resulted in the formation of multiple ply cracks in the 90° Co layer within the first few cycles, similar to the behavior known for cross-ply laminates [36]. They occurred at a regular spacing and were considerably large with the ply thickness being approximately 0.32 mm. With increasing numbers of cycles, they grew into the matrix and triggered delamination between the 0° and the 90° ply. The evolution of crack density that is typical for DiCo SMC (cf. Fig. 12) could not be observed in the DiCo ply of [0/90/DiCo/90/0] specimens. This means, that the full potential of the DiCo ply could not be exploited. The stiffness degradation behavior generally improved compared to DiCo SMC but was still inferior to that of [0/DiCo/0] specimens.

6. Conclusions

For a hybrid composite consisting of a discontinuous glass fiber SMC core and unidirectional carbon fiber reinforced face plies, effects of hybridization were more pronounced under fatigue loading than under monotonic loading. Compared to DiCo SMC, tensile strength of [0/DiCo/0] specimens increased by 126% and 92% at quasi-static and fatigue strain rate, respectively. In contrast, fatigue strength of [0/DiCo/0] specimens at $2.6 \cdot 10^6$ cycles increased by 209% compared to DiCo SMC. This resulted from altered damage evolution with the damage behavior being dominated by the Co ply under monotonic loading and by the DiCo ply under fatigue loading. The strain-life behavior of the hybrid composite was superior to both of its constituents in the high cycle fatigue range, which means that a true hybridization effect with the hybrid exceeding the properties of each constituent is observed. Hybridization effects under cyclic loading were less pronounced, when the unidirectional continuous reinforcement was replaced by a cross-ply reinforcement. In the latter case, tensile strength at quasi-static and fatigue strain rate and fatigue strength increased by 94%, 71% and 85% compared to DiCo SMC, respectively. The early initiation and growth of 90° ply cracks resulted in stronger localization of damage and thus in
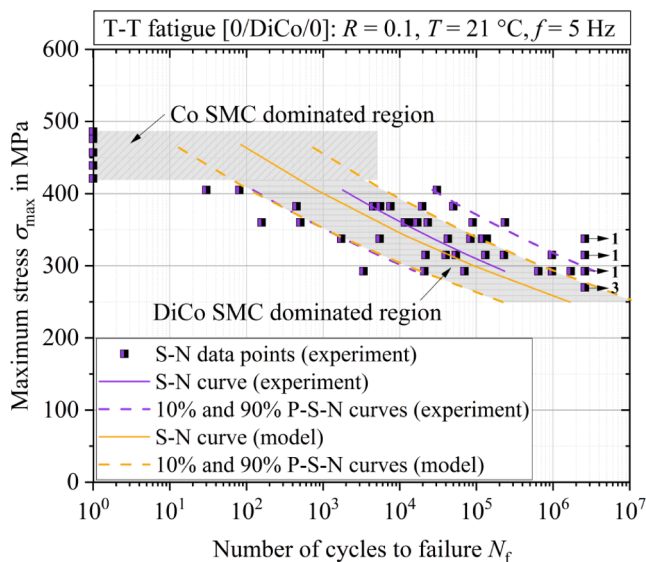

Fig. 15. Analytical estimation of the fatigue life of [0/DiCo/0]. The purple lines depict the S-N curve of [0/DiCo/0] specimens (solid line) obtained from experimental results via linear regression and corresponding 10% and 90% P-S-N curves (dashed lines), whereas yellow lines depict the results obtained with an empirical modeling approach. The grey shaded areas distinguish between the predominant damage mechanisms in the corresponding stress ranges. (For interpretation of the references to colour in this figure legend, the reader is referred to the web version of this article.)

reduced fatigue resistance.

The results obtained in this study underline the potential of hybrid continuous-discontinuous fiber-reinforced SMC composites for applications subjected to cyclic loading. While effects of hybridization were investigated exclusively under tension–tension load in this study, more application related loading conditions including cyclic bending at alternating frequency and temperature need to be considered for future studies.

Declaration of Competing Interest

The authors declare that they have no known competing financial interests or personal relationships that could have appeared to influence the work reported in this paper.

Acknowledgments

References

[1] Böhlke T, Henning F, Hrymak A, Kärger L, Weidenmann KA, Wood JT. Continuous–Discontinuous Fiber-Reinforced Polymers. München: Carl Hanser Verlag GmbH & Co. KG; 2019.

[2] Gardiner G. JEC 2017 – Aiming for Industrialization. [accessed 29.12.2020]; Available from: https://www.compositesworld.com/articles/jec-2017-aiming-for-industrialization.

[3] Bruderick M, Denton D, Shinedling M, and Kiesel M. Applications of carbon fiber SMC for the Dodge Viper. In: Proceedings to Automotive Composites Conference \& Exhibition (ACCE), Detroit; 2013.

[4] Trauth A, Weidenmann KA. Continuous-discontinuous sheet moulding compounds – effect of hybridisation on mechanical material properties. Compos Struct 2018; 202:1087–98. https://doi.org/10.1016/j.compstruct.2018.05.048.

[5] Trauth A, Weidenmann KA, Altenhof W. Puncture properties of a hybrid continuous-discontinuous sheet moulding compound for structural applications. Compos B Eng 2019;158:46–54. https://doi.org/10.1016/j.compositesb.2018.09.035.

[6] Trauth A. Characterisation and Modelling of Continuous-Discontinuous Sheet Moulding Compound Composites for Structural Applications. Karlsruhe: KIT Scientific publishing; 2020.

[7] Hayashi T. On the improvement of mechanical properties of composites by hybrid composition. In: Proceedings of the 8th International Reinforced Plastics, p. 149–152.

[8] Swolfs Y, Gorbatikh L, Verpoest I. Fibre hybridisation in polymer composites: a review. Compos A Appl Sci Manuf 2014;67:181–200.

[9] Bücheler D, Henning F. Hybrid resin improves position and alignment of continuously reinforced prepreg during compression co-molding with sheet molding compound. In: Proceedings of the 17th European Conference on Composite Materials, Munich, Germany; 2016, p. 26–30.

[10] Owen MJ. Static and Fatigue Strength of Glass Chopped Strand Mat/Polyester Resin Laminates. In: Sanders BA, editor. Short Fiber Reinforced Composite Materials. 100 Barr Harbor Drive, PO Box C700, West Conshohocken, PA 19428-2959: ASTM International; 1982, 64-64-21.

[11] Wang SS, Chim E-M. Fatigue damage and degradation in random short-fiber SMC composite. J Compos Mater 1983;17(2):114–34. https://doi.org/10.1177/002199838301700203.

[12] Shirinbayan M, Fitoussi J, Meraghni F, Surowiec B, Laribi M, Tcharkhtchi A. Coupled effect of loading frequency and amplitude on the fatigue behavior of advanced sheet molding compound (A-SMC). J Reinf Plast Compos 2017;36(4): 271–82. https://doi.org/10.1177/0731684416682853.

[13] Talreja R. Fatigue of composite materials: damage mechanisms and fatigue-life diagrams. Proc R Soc Lond A 1981;378(1775):461–75. https://doi.org/10.1098/rspa.1981.0163.

[14] Gamstedt EK. Effects of debonding and fiber strength distribution on fatigue-damage propagation in carbon fiber-reinforced epoxy. J Appl Polym Sci 2000;76 (4):457–74.

[15] Kawai M, Yano K. Anisomorphic constant fatigue life diagrams of constant probability of failure and prediction of P-S–N curves for unidirectional carbon/epoxy laminates. Int J Fatigue 2016;83(163–186):323–34. https://doi.org/10.1016/j.ijfatigue.2015.11.005.

[16] Sørensen BF, Goutianos S. Micromechanical model for prediction of the fatigue limit for unidirectional fibre composites. Mech Mater 2019;131:169–87. https://doi.org/10.1016/j.mechmat.2019.01.023.

[17] Schulte K, Baron Ch. Schädigungsentwicklung bei Ermüdung verschiedener CFK-Laminate. Mat-wiss u Werkstofftech 1987;18(4):103–10. https://doi.org/10.1002/mawe.19870180404.

[18] Reifsnider KL, Henneke EG, Stinchcomb WW, Duke JC. DAMAGE MECHANICS AND NDE OF COMPOSITE LAMINATES. In: Elsevier, editor. Mechanics of Composite Materials. Elsevier; 1983, p. 399–420.

[19] Talreja R. Transverse cracking and stiffness reduction in composite laminates. J Compos Mater 1985;19(4):355–75. https://doi.org/10.1177/002199838501900404.

[20] Riegner DA, Sanders BA. A characterization study of automotive continuous and random glass fiber composites. Report GMMD 1979;23.

[21] Kundrat R, Joneja S, Broutman LJ. Fatigue damage studies in high strength sheet-molding compound fiberglass composites. Polym Compos 1982;3(3):105–12. https://doi.org/10.1002/pc.750030302.

[22] Springer GS. Effects of temperature and moisture on sheet molding compounds. J Reinf Plast Compos 1983;2(2):70–89. https://doi.org/10.1177/073168448300200201.

[23] Dickson RF, Fernando G, Adam T, Reiter H, Harris B. Fatigue behaviour of hybrid composites. J Mater Sci 1989;24(1):227–33. https://doi.org/10.1007/BF00660958.

[24] Hofer KE, Stander M, Bennett LC. Degradation and enhancement of the fatigue behavior of glass/graphite/epoxy hybrid composites after accelerated aging. Polym Eng Sci 1978;18(2):120–7. https://doi.org/10.1002/pen.760180210.

[25] DIN EN ISO 527-5. Kunststoffe - Bestimmung der Zugeigenschaften: Teil 5: Prüfbedingungen für unidirektional faserverstärkte(527-5). Berlin: Deutsches Institut für Normung e.V., Beuth Verlag GmbH; 2010.

[26] DIN EN ISO 527-4. Kunststoffe - Bestimmung der Zugeigenschaften: Teil 4: Prüfbedingungen für isotrop und anisotrop faserverstärkte Kunststoffverbundwerkstoffe(527-4). Berlin: Deutsches Institut für Normung e.V., Beuth Verlag GmbH; 1997.

[27] Le T-H, Dumont P, Orgéas L, Favier D, Salvo L, Boller E. X-ray phase contrast microtomography for the analysis of the fibrous microstructure of SMC composites. Compos A Appl Sci Manuf 2008;39(1):91–103. https://doi.org/10.1016/j.compositesa.2007.08.027.

[28] ISO 13003. Fibre-reinforced plastics - Determination of fatigue properties under cyclic loading conditions(13003). Geneva, Switzerland: International Organization for Standardization; 2003.

[29] DIN EN ISO 527-1. Kunststoffe - Bestimmung der Zugeigenschaften - Teil1 Allgemeine Grundsätze(527-1). Berlin: Deutsches Institut für Normung e.V., Beuth Verlag GmbH; 2012.

[30] Quaresimin M, Carraro PA, Mikkelsen LP, Lucato N, Vivian L, Brøndsted P, et al. Damage evolution under cyclic multiaxial stress state: A comparative analysis between glass/epoxy laminates and tubes. Compos B Eng 2014;61:282–90.

[31] Mandell JF, Meier U. Effects of Stress Ratio, Frequency, and Loading Time on the Tensile Fatigue of Glass-Reinforced Epoxy. In: O'Brien TK, editor. Long-Term Behavior of Composites. 100 Barr Harbor Drive, PO Box C700, West Conshohocken, PA 19428-2959: ASTM International; 1983.

[32] Denton DL. Mechanical properties characterization of an SMC-R50 Composite. SAE Trans 1979:2283–94.

[33] Zoltek Corporation. Technical Datasheet - Zoltek PX35 Continuous Tow.

[34] Dugin NA, Zaboronkova TM, Krafft C, Belyaev GR. Carbon-based composite microwave antennas. Electronics 2020;9(4):590. https://doi.org/10.3390/electronics9040590.

[35] Mandell JF. Fatigue behavior of short fiber composite materials. Fatigue Compos Mater 1991:231–337.

[36] Highsmith AL, Reifsnider KL. Stiffness-Reduction Mechanisms in Composite Laminates. In: Reifsnider KL, editor. Damage in Composite Materials: Basic Mechanisms, Accumulation, Tolerance, and Characterization. 100 Barr Harbor Drive, PO Box C700, West Conshohocken, PA 19428-2959: ASTM International; 1982, 103-103-15.